VII International Conference on Computational Methods in Marine Engineering
MARINE 2017
M. Visonneau, P. Queutey and D. Le Touzé (Eds)

DEVELOPMENT OF A FLUID STRUCTURE COUPLING FOR COMPOSITE TIDAL TURBINES AND MARINE PROPELLERS

POL MULLER* AND FABIAN PÉCOT*

* DCNS Research / SIREHNA
Technocampus Océan
Rue de l'Halbrane, 44340 Bouguenais, France
e-mail: pol.muller@sirehna.com, fabian.pecot@sirehna.com

Key words: Fluid Structure Coupling, Propeller, Tidal Turbine, Composite

Abstract. The recent strong development of composite blades for propellers and tidal turbines has been driven both by the reduction of mass compared to metallic materials and by the impact of the deformations of blades on the increase of their performances (as shown for instance in [1]). The gain in performances concerns the efficiency of the propeller or turbine, the mitigation of the risk of cavitation and, by extension, the reduction of noise and vibrations. In order to help the designer to make the appropriate choices during the early stages of the design, new numerical tools like a fluid-structure coupling for "heavy" fluid are necessary in addition to existing numerical and experimental methods. This paper focuses on the development of such a fluid-structure coupling algorithm for tidal turbines and marine propellers. The main objectives for the blades are: to get an accurate estimation of the deformations and stresses under a hydrodynamic load, to include these predictions in a design process in order to increase efficiency and reliability and finally to optimize the hydrodynamic shape and inner structure. In terms of software development the main target is to provide an efficient tool which can be integrated in an optimisation environment for preliminary to intermediate design phases, therefore with low resource consumption, fast execution time, easy file setup and fully scripted for an automated execution in command line.

1 FLOW SOLVER

The flow solver used by the present coupling algorithm is PROCAL, a 3D Boundary Element Method (BEM) based on potential flow theory, developed by the CRS organisation [2]. The PROCAL code computes the wetted and cavitating potential flow around blade geometries operating in an input wake field. It solves the steady or unsteady potential flow problem for an arbitrary number of rotating and non-rotating surfaces. The lifting bodies generate a wake geometry which can be described by an input mesh or by wake generation routines which have been implemented for rotating bodies such as propeller or tidal turbine blades. In order to account for viscous effects which are not considered in a potential flow theory, a post-processing computation of the forces is made using empirical corrections based on flat plate skin friction coefficients.

Assuming the flow to be incompressible and irrotational, the flow velocity V can be defined as a function of a potential Φ as in (1). This potential is split into two contributions (2) where

φ_∞ is the potential of the undisturbed flow, and φ is the disturbance potential to be solved, which satisfies the Laplace equation (3). The boundaries of the domain consist of the blade and hub surfaces S_B and S_H on which the kinematic boundary condition (4) is applied.

$$\vec{V} = \vec{\nabla}\Phi \tag{1}$$

$$\Phi = \varphi_\infty + \varphi \tag{2}$$

$$\nabla^2\varphi = 0 \tag{3}$$

$$\frac{\partial\varphi}{\partial n} = -\vec{V_\infty}.\vec{n} \tag{4}$$

At infinity, the disturbance due to the body on the flow vanishes to zero. In addition, the lifting surfaces are generating a wake surface S_W which consists of vortex sheets being shed from the trailing edges. The normal velocity is null on this surface and the pressure is continuous across it.

Assuming that the potential is null within the bodies, i.e. within the surfaces S_B and S_H, the second Green's theorem applied to the computational domain shows that the resolution of the flow can be reduced to the unknowns at the boundaries only (5).

$$\varphi_p = \frac{1}{2\pi}\int_{S_B \cup S_H}\left[\varphi_q \frac{\partial}{\partial n_q}\left(\frac{1}{R_{p,q}}\right) - \frac{\partial\varphi_q}{\partial n_q}\frac{1}{R_{p,q}}\right]dS \tag{5}$$

Without going into the mathematical resolution of this equation and its implementation in PROCAL, which can be found in [3], we can tell that the strengths of the singularities for the sources and potentials are assumed to be constant on each panel. A mesh is built with quadrilateral panels on the blade and hub surfaces (Figure 1).

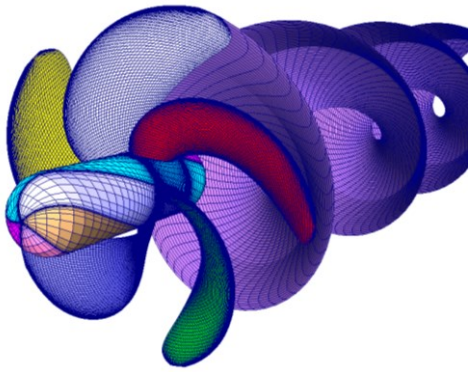

Figure 1: Example of a panel mesh on a propeller including only one blade wake surface for better visibility.

This flow solver has been extensively validated within CRS working groups for a large range of propellers with various shapes, number of blades and diameters, for model scale and full scale. Although it is suitable for computing the flow on blades either in uniform inflow or in a

non-uniform wakefield, it is used in the present coupling algorithm only in axisymmetric inflow.

The coordinate system used by PROCAL and recommended by the International Towing Tank Conference (ITTC) is chosen as the general coordinate system for the present coupling algorithm. The first axis X is longitudinal (along the rotation axis) towards upstream, the third axis Z is coincident with the blade reference line toward the blade tip and the second axis Y completes the right handed reference frame, see Figure 2.

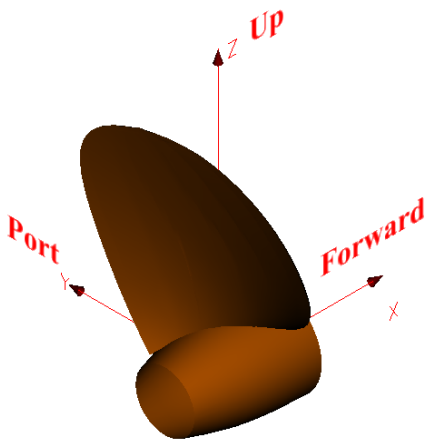

Figure 2: Propeller reference system, *in* [4].

2 STRUCTURE SOLVER

The commercial solver ABAQUS 6.13 [5] distributed by "Dassault Systèmes" is used in the present coupling algorithm.

2.1 Type of elements

Various elements can be applied to describe the structure: volume elements, shells or thick shells. Considering that the propeller blade is made of composite material distributed in thin layers (plies) with orthotropic properties, it is not easily described by volume elements which should have the same thickness as each ply or group of plies with similar properties. In order to grant as much freedom as possible to the designer, the algorithm should not assume that the plies can be subdivided into groups with similar properties, but should consider each ply separately. The thickness of such plies can easily be below 0.5 mm which implies that the total number of elements will be incompatible with a low computer resource consumption and with low computation time. On the other hand, the volume elements are an adequate representation of the actual geometry, both in terms of inner structure and in terms of outer shape. This outer layer is the boundary between hydrodynamics and structure, where the information is exchanged between the flow solver and the structure solver (see chapter 3). Therefore, it is of main interest for the algorithm to preserve the geometry of this boundary.

The shell elements provide an excellent efficiency in terms of computer resources because the number of elements is much less than when using volume elements, and because the mathematical modelling of the material is simplified. In this case, the blade is assumed to be

infinitely thin and is replaced by its mid plane. The formulation of shell sections in ABAQUS can handle the distribution of plies in each element by describing the ply material, orientation and thickness. Unfortunately the geometrical link between the shell and the outer boundaries of the structure is not represented. This means that the algorithm has to transfer the hydrodynamic pressure applied on the suction and pressure sides to the shell elements and in return has to compute the deformation of the outer surfaces of the blade. The transfer of pressure can be relatively easily handled with projection but the deformation of the outer surface based on the shell deformation can introduce uncertainties, especially in areas with large thickness or curvature variations, such as leading edges and trailing edges.

A reasonable intermediate between volume and shell elements is the thick shell element in ABAQUS which combines a low number of elements for a complete description of the blade, with simplified mathematical description of the material, and an element which has actual nodes on the outer surface of the blade. The transfer of information such as pressure and deformations on the faces is therefore possible without any specific pre/post processing and the computation time remains low enough to be used in an optimisation environment. One remaining issue is that the material has to be applied as a single stack on the element. It is well supported by ABAQUS as presented on Figure 3, but the user has to specify the exact stack of plies. As the thickness of the blade is not constant, the number of plies varies from one element to another so the user almost has to define a new stack for each element. This can be easily tackled with an automated pre-processing based on the actual element thickness, directly computed from the node coordinates, which selects the appropriate plies to be applied to the element. This type of element has been selected for the modelling of the blade structure within the coupling algorithm.

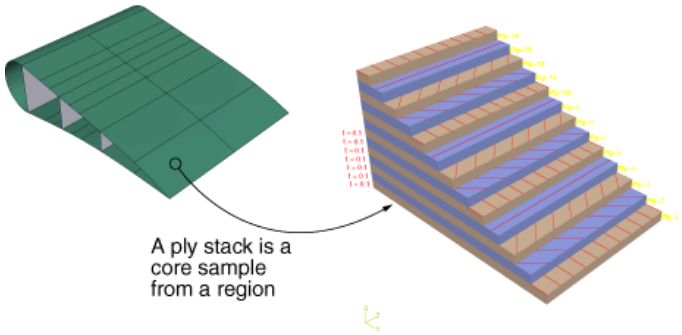

Figure 3: Example of ply stack representation in ABAQUS, *in* [5].

2.2 Definition of the material

The composite material is supposed to be orthotropic and distributed in plies. The target material is a Fibre-Reinforced Plastic, such as CFRP or GFRP (carbon or glass fibres). In ABAQUS this type of material can be defined as a stack of plies with variable mechanical properties, thicknesses and orientations of the fibres. It is therefore possible to define a stack for a given thick shell element. The orthotropic mechanical properties of the material are given as inputs together with the thickness of each ply. The main issue concerns the orientation of the material within the ply. A detailed computation of an actual composite blade would need to use

a wrapping tool which can be included in some CAD suites. The typical purpose of such a tool is both to provide a local coordinate system (LCS) of a ply for any point in the structure and to check that the skew and twist of the fibres will be acceptable in areas with large curvatures. As the present algorithm is dedicated to optimisation tasks in a fully automated environment, the usage of such a wrapper is not realistic. One has to define the LCS according to a chosen convention. A literature review does not emphasize a clear unique convention. For instance in [6] the fibre directions are defined in the local spanwise coordinate system, whereas in [7] the LCS is the same as the general coordinate system. The main consequence is that, for a given fibre orientation, the resulting model with these two different conventions will not be identical and may produce different results in terms of mechanical behaviour (stresses, deformations and hydrodynamic forces). For the present coupling algorithm another convention has been used, taking into account the strength and weaknesses of the above described conventions. It is not likely that a fibre with a zero degree orientation will follow the local spanwise direction, especially for high skew blades. This would also results in high skew of the fibre which is not favourable for the strength of the material. On the other hand it is likely that the fibre will be twisted or skewed in order to follow the general shape of the blade. A unique LCS is therefore not chosen. The convention used in the present algorithm is such that the third axis of the LCS is the normal to the shell element towards upstream, the first axis is in the XZ plane of the general coordinate system and the second axis completes the right handed reference frame, see Figure 2. It is a balance between a global coordinate system and a system purely based on a blade element geometry.

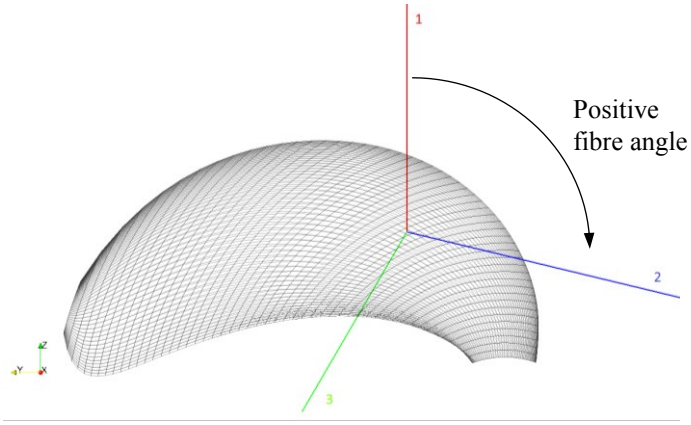

Figure 4: Local coordinate system for the definition of the fibre orientation in a ply.

3 COUPLING ALGORITHM

The general algorithm is based on successive iterations on the displacement of the mesh nodes and of the pressure on the mesh panels, until convergence, as presented on Figure 5. It is solved in static condition, i.e. in an axisymmetric inflow, without any influence of a dynamic deformation of the blade or of added mass.

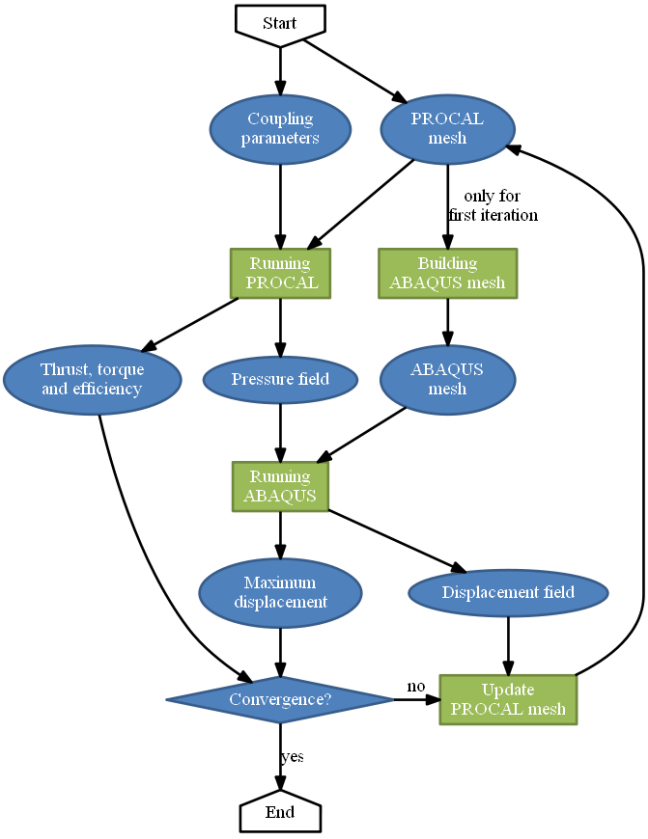

Figure 5: General algorithm.

3.1 Mesh

As already mentioned the pressure and displacement are exchanged over a boundary surface between fluid and structure which is the envelope of the blade, namely its pressure and suction sides. It is therefore important to preserve as much as possible the information exchanged on this surface in order to limit any numerical discrepancy that would be introduced by interpolations or extrapolations. The simplest solution to cope with this potential issue is to use a coincident mesh both for the BEM method and for the structure solver. The hydrodynamic pressure is computed by the flow solver at the panel centres: this information can be directly transferred to the facets of the structure elements. In return the deformations of the structure elements are computed at the elements nodes: this can be directly used to update the mesh read by the flow solver. In consequence the meshes used by the flow and structure solvers have at least their surface nodes in common from the first to the final iteration. There is no need to build a new mesh after each iteration which saves computation time, prevents interpolations and preserves the history of stresses in structure elements. One can also easily check that, at each iteration, on the one hand the pressure computed by the flow solver is the same as the one used as input for the structure solver, and on the other hand that the node coordinates of the structure and fluid meshes are the same. In order to keep the history of stresses in structure elements from one iteration to the following, the structure computation for an iteration is restarted from the previous solution simply by updating the input pressure field.

3.2 Code implementation

The implementation of the coupling algorithm has been made using python scripts. These scripts can handle each step of the computation process in an automated way. The steps covered are: meshing of the blade for the flow solver starting from its geometric description, building the structure mesh, applying the material on the structure elements, building the control scripts for the flow solver and for the structure solver, running the solvers, reading and converting the pressures and displacement from one solver to the other, updating the fluid mesh and finally check the convergence. The convergence of the algorithm is based both on hydrodynamic forces (thrust and torque on the blades) and on structure displacements. All relevant parameters of the simulation have been gathered in a single general input file which has to be filled by the user, and are then allocated to the corresponding input files of the solvers. As a matter of fact isotropic materials are considered as a special case of orthotropic materials therefore the coupling algorithm can handle metallic materials for instance.

In terms of computing performances on a desktop computer, one iteration takes between 1 minute for a low skew blade (up to a skew angle of 15 degrees with 1 500 to 2 000 panels on the blade surface) up to 5 minutes for a high-skewed blade (with skew angle higher than 45 degrees and 10 000 panels on the blade surface). The computation time is almost equally divided between the flow resolution and the structure deformation. The targets in terms of software development are therefore achieved: the tool can be fully scripted for an automated execution in command line, with low resource consumption, fast execution time and easy file setup.

4 TEST CASE

The test case which has been selected is described in [7] and [8]. It is based on the high-skew propeller DTNSRDC 4498 [9] with 5 blades and a diameter of 1 foot (Figure 6). Starting from the original geometry, [7] and [8] define a material (CFRP) with two different orientation sequences. Based on deformation computations, they define a new "pre-deformed" geometry with one orientation sequence, which should have the original DTNSRDC 4498 shape under a given hydrodynamic load. This sums up to a total of three different blades which are summarized in the Table 1. For a complete description of the orientation sequence convention, please refer to [8]. One should emphasize that the orientation sequence of the 4498_1 propeller produces deformations which are close to an equivalent isotropic material, whereas the second orientation sequence gives a clear dominant direction of deformations.

Reference results of propellers 4498_1, 4498_2 and 4498_3 are presented in [8]. They consist of both computation results and experimental measurements of thrust coefficient, torque coefficient and blade deformation for various inflow velocities and rotation speeds, for a total of 54 different cases.

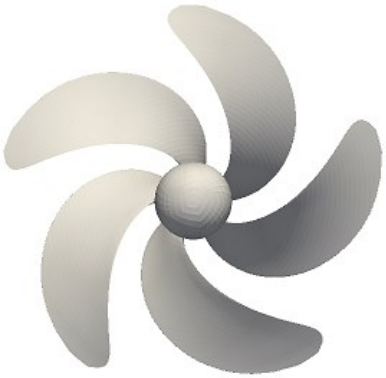

Figure 6: Overview of the 4498 propeller.

Table 1: Summary of test cases

Case id	Orientation sequence	Pre-deformed
4498_1	[-45°$_2$/90°$_2$/45°$_2$/0°$_2$/-45°$_2$/90°$_2$/45°$_2$/0°$_2$/-45°$_2$/90°$_2$/45°$_2$/0°$_2$]s	No
4498_2	[45°$_2$/90°$_2$/45°$_2$/45°$_2$/45°$_2$/45°$_2$/0°$_2$/0°$_2$/0°$_2$/0°$_2$/0°$_2$/45°$_2$]s	No
4498_3	[45°$_2$/90°$_2$/45°$_2$/45°$_2$/45°$_2$/45°$_2$/0°$_2$/0°$_2$/0°$_2$/0°$_2$/0°$_2$/45°$_2$]s	Yes

5 RESULTS

The following results have been obtained after a proper mesh independence study, for the flow solver, the structure solver and the coupling of both. It appears that the necessary mesh refinement is higher for the convergence of the structure deformations than for the convergence of the hydrodynamic forces on this specific case.

5.1 Blade deformations

In order to compensate for any offset that could introduce unexpected inaccuracy in the experimental setup, the deformations are compared for each propeller versus the deformations of the 4498_1. The description of the experimental setup for measuring the blade deformations is not detailed on the possible gap of the thrust bearing which may introduce offsets into the blade deformation measurement along the axial direction. These deformations are measured in this direction only by means of video cameras which are used to track the displacement of markers on the leading and trailing edges of the blades, at 95% of the blade radius. Results are presented in Figure 9. For the leading edge (two first rows of the figure) the order of magnitude of the difference with experimental measurements is less than 0.2 mm and the sorting of the blades by order of deformation intensity is preserved, which is of major importance for an optimisation study. On the other hand the results are less satisfactory on the trailing edge (two last rows of the figure): both the order of magnitude of the displacement and the sorting are significantly different from the leading edge results. It is important to notice that the trailing edge thickness (up to 80% of the chord length) is less than 1 mm which means that the number of plies in this area is 2 or 4. There is a significant manufacturing uncertainty in this area. In addition the theoretical profile used in the computation has a zero thickness at the trailing edge which is of course not feasible in reality. These manufacturing uncertainties on the trailing edge thickness may produce significant differences in terms of deformations.

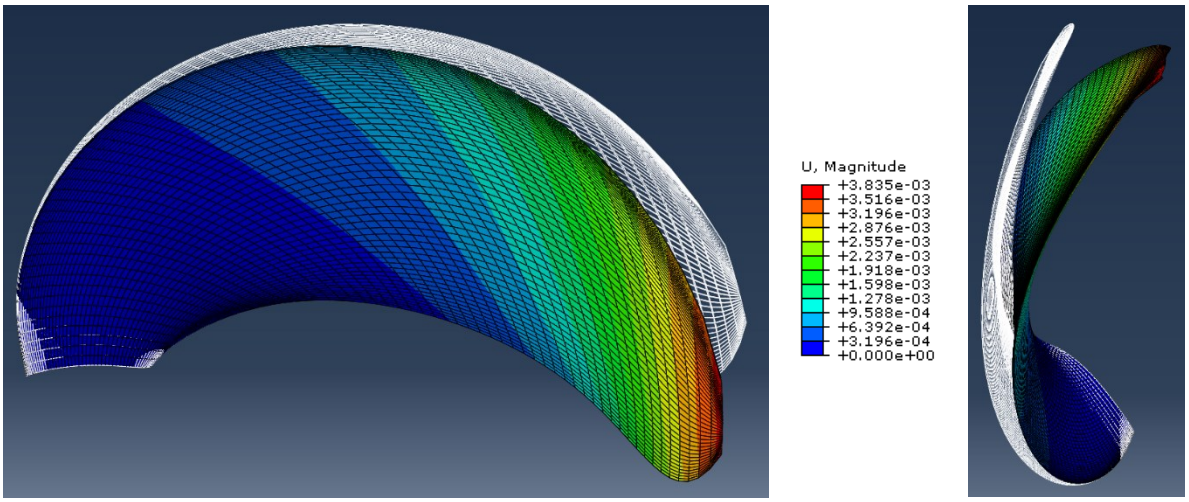

Figure 7: 4498_3 blade deformations at J=0.600 (20Hz) seen from the suction side (left) and from the leading edge (right), coloured by deformation amplitude and magnified x10.

5.2 Hydrodynamic forces

For the 4498_1 propeller, with an orientation sequence such that the material is almost isotropic, the hydrodynamic forces induced by the deformations at the design point are within 1 to 2% on thrust coefficient compared to experimental results, and 1 to 10% for torque coefficient, depending on the rotation rate.

For the 4498_2 propeller, the thrust and torque coefficients induced by the deformations at the design point are within 2% for the highest rotation rate (13Hz) and 10 to 15% for the lowest rotation rate (7Hz). For the latter case one can notice that the Reynolds number at 0.7R is well below the recommended values by the ITTC. The flow on the blade should be mostly laminar which is not accurately resolved. It is also possible that the actual material orientation is inadequately represented by the chosen LCS convention.

For the 4498_3 propeller, the results are in the same order of magnitude as for the 4498_2 propeller.

Examples of open water results (best and worse) are presented on Figure 10.

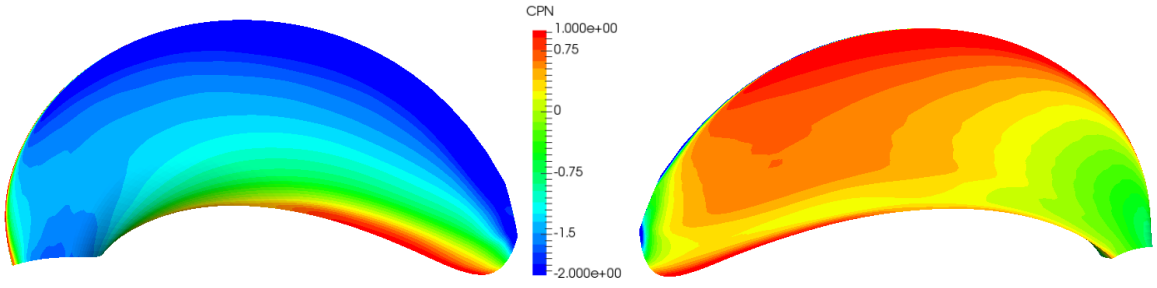

Figure 8: Pressure field on the 4498_3 blade at J=0.600 (20Hz).

6 CONCLUSIONS AND PERPECTIVES

The main objectives of the coupling algorithm are split into computing performances, user friendliness, and result accuracy. The computing performances are reasonable enough to be integrated in an optimisation environment where a large number of blade variants should be computed, both in terms of geometry modifications and material stacking sequences. The user friendliness is also very decent as there is only one main control text file with less than a dozen of parameters to fill in. This can also be filled or modified in an automated way within an optimisation environment. The results accuracy need to be improved and extended to other tests cases. The identified sources of discrepancies are: uncertainties on the actual geometry of the manufactured propeller model, small diameter (1 foot) which implies small deformations, high-skewed blade and laminar flow which are difficult to compute with BEM software, usage of thick shell structure elements which are simplified compared to volume elements, possible discrepancies in the fibre orientation definition. Although this coupling algorithm has some perfectible features, it is still possible to use it in a preliminary or intermediate design phase, with optimisation of the blade geometry and fibre orientations.

This coupling algorithm is dedicated to propeller and tidal turbine blades in an axisymmetric inflow. An extension to a non-uniform inflow, such as a ship wake field of a current inflow profile close to the sea bed would extend the possible use of this tool.

REFERENCES

[1] *The Propulsion Committee - Final report and recommendations to the 24th ITTC*, ITTC 2005.
[2] The Cooperative Research Ships (CRS) – http://www.crships.org/.
[3] Bosschers, J. *PROCAL v2.0 theory manual*. MARIN report Report 20834-7-RD (2009).
[4] *Dictionary of Hydromechanics*, ITTC 2014.
[5] ABAQUS version 6.13 Documentation (2013), Dassault Systèmes Simulia Corp., Providence, RI, USA.
[6] Young, Y. L., *Fluid–structure interaction analysis of flexible composite marine propellers.* Journal of Fluids and Structures (2008) **24**:799-818.
[7] Lee, Y. J. and Lin, C. C., *Optimized design of composite propeller*. Mechanics of advanced materials and structures (2004) **11**:17-30.
[8] Lin, C. C., Lee, Y. J. and Hung, C. S, *Optimization and experiment of composite marine propellers*. Composite Structures (2009) **89:**206-215.
[9] J. J. Nelka, *Experimental evaluation of a series of skewed propellers with forward rake: openwater performance, cavitation performance, field-point pressures, and unsteady propeller loading*, DTNSRDC Report 4113 (1974).

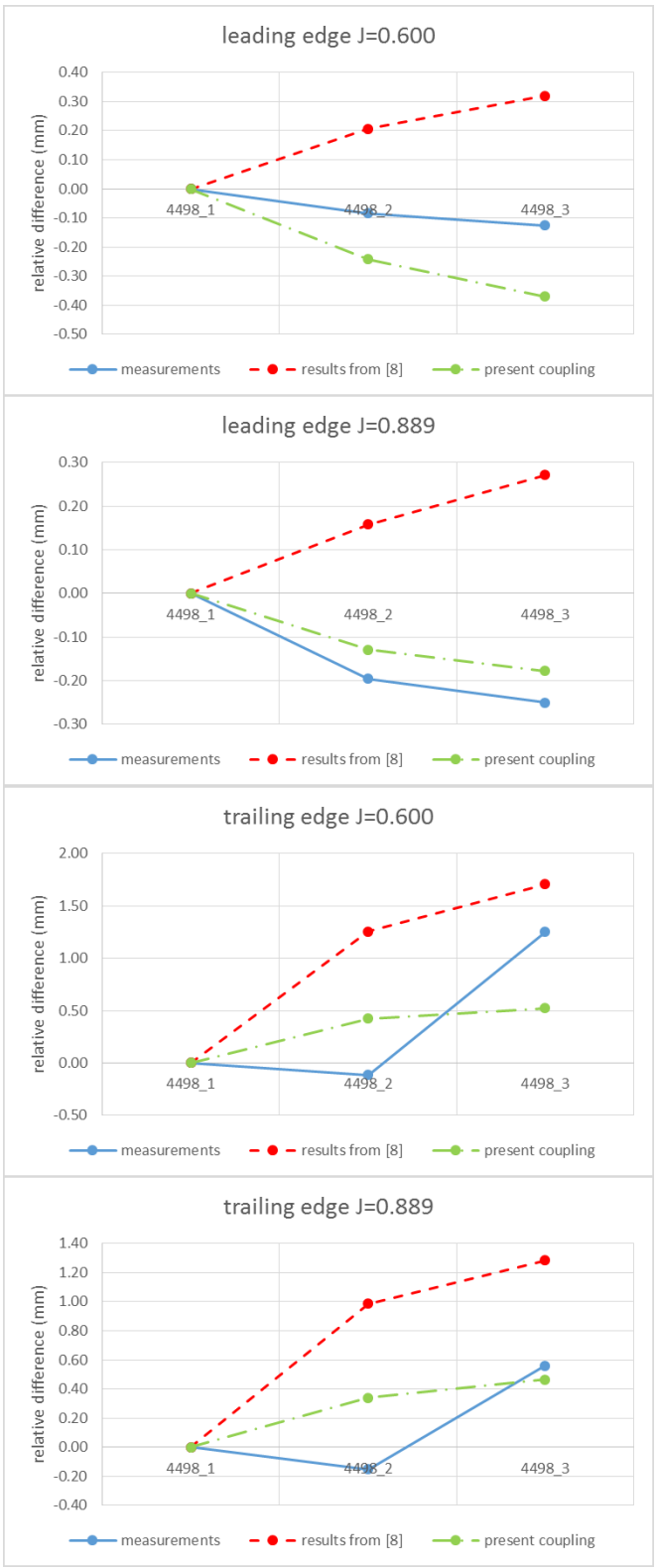

Figure 9: Overview of the blade deformations at 95% of the radius.

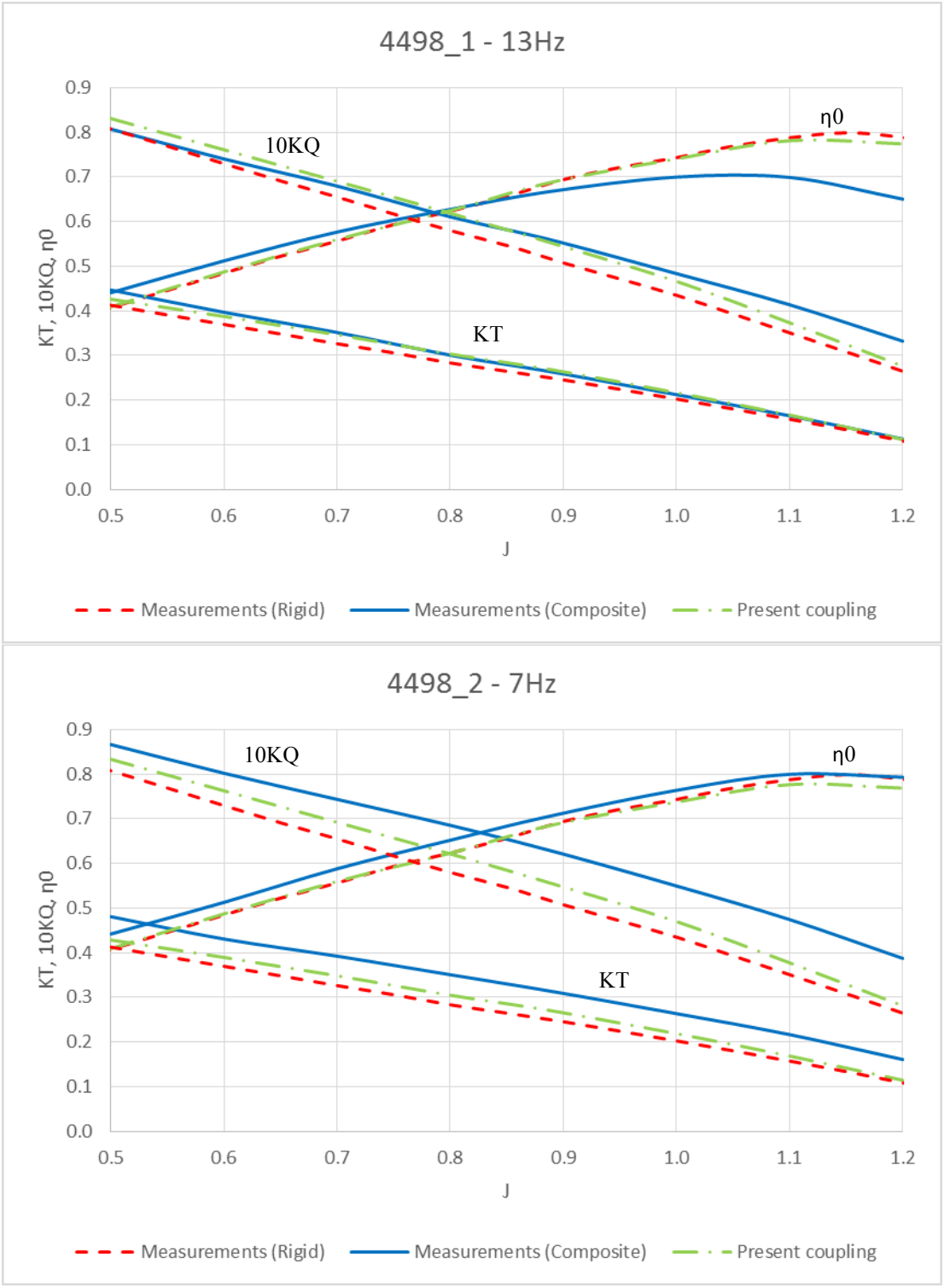

Figure 10: Examples of open water results.